

[Ni(H₂O)₆](NO₃)₂·(15-crown-5)·2H₂O: three phase transitions and an intermediate modulated phase stable over a range of ca 40 K

Maxime A. Siegler,* Xiang Hao,
Sean Parkin and Carolyn Pratt
Brock*

Department of Chemistry, University of
Kentucky, Lexington, KY 40506-0055, USA

Correspondence e-mail: xray@jhu.edu,
cpbrock@uky.edu

Received 8 September 2011

Accepted 31 October 2011

In the range 308–90 K single crystals of [Ni(H₂O)₆](NO₃)₂·(15-crown-5)·2H₂O continue to diffract well as they undergo three phase transitions. Structures have been determined at 28 different temperatures; data were collected at six more but could not be refined satisfactorily. The transitions identified structurally are in good agreement with those found by thermal analysis. Phase I (above ca 292 K; *I*2/*m*, *Z* = 2, *Z*' = $\frac{1}{4}$) is disordered because the 15-crown-5 molecule is located on a *2/m* site. Phase II (ca 292–248 K; *P*2₁/*m*, *Z* = 2, *Z*' = $\frac{1}{2}$) is less disordered. Phase III (ca 248–208 K; *B*2₁, *Z* = 28, *Z*' = 7 in a commensurate approximation) is modulated with some regions resembling phase II and the rest resembling the fully ordered phase IV (*P*2₁/*c*, *Z* = 4, *Z*' = 1) that is stable below ca 208 K. The modulated structure could be determined well because crystals flash-cooled to 90 K usually retain the phase III structure. The unusual phase III may be a consequence of the differing thermal contraction of two types of alternating layers, one composed of neutral 15-crown-5 molecules and the other composed of the cations, anions and lattice water molecules, which form a hydrogen-bonded network. The two kinds of layers are linked by O_{ether} ··· H₂O_{axial}—Ni hydrogen bonds.

1. Introduction

The compound [Ni(H₂O)₆](NO₃)₂·(15-crown-5)·2H₂O (referred to hereafter as NiW6-2W) was made during attempts (ultimately successful; Siegler *et al.*, 2008) to synthesize [Ni(H₂O)₂(15-crown-5)](NO₃)₂. Crystals of NiW6-2W had been studied previously at 173 K by Steed *et al.* (2001), who found a *P*2₁/*c*, *Z*' = 1 structure (refcode XEMGIF in the CSD; Allen, 2002). The crystals we first studied at room temperature had an *I*2/*m*, *Z*' = $\frac{1}{4}$ structure, and most crystals that were flash-cooled to 90 K had an unusual, modulated structure that we described in *B*2₁ with *Z*' = 7. We decided to make a detailed study of this apparent phase sequence.

A sequence of three first-order phase transitions (see Fig. 1) connecting four phases, hereafter designated as I (at room temperature) through II and III to IV (the XEMGIF structure) was found. Single crystals can be taken through these transitions without any apparent damage or loss of diffracting power. The phase sequence is the same for heating as for cooling. The most surprising feature of the phase sequence is the presence of an unusual modulated, intermediate phase (phase III) stable over ca 40 K. While the modulations are probably incommensurate, the structure is described in this first report in an approximate commensurate supercell with *Z*' = 7. In this phase III there are regions similar to the disordered phase II (*P*2₁/*m*, *Z*' = $\frac{1}{2}$) that is stable at somewhat higher temperatures; these regions alternate periodically with

regions that are similar to the ordered phase IV ($P2_1/c$, $Z' = 1$) stable at yet lower temperatures. If a crystal is cooled very rapidly from room temperature to 90 K it usually, although not always, becomes stuck in phase III, which can therefore be studied at 90 K, where it remains metastable, at least long enough that data can be collected.

All phases are dihydrated co-crystals of $[\text{Ni}(\text{H}_2\text{O})_6](\text{NO}_3)_2$ and 15-crown-5. The hexaaquanickel(II) ions and the crown molecules form hydrogen-bonded chains (see Fig. 2). These chains are cross-linked by hydrogen bonds formed between ligand water molecules, lattice water molecules and nitrate anions (see Fig. 3). The hydrogen-bonded layers alternate (see

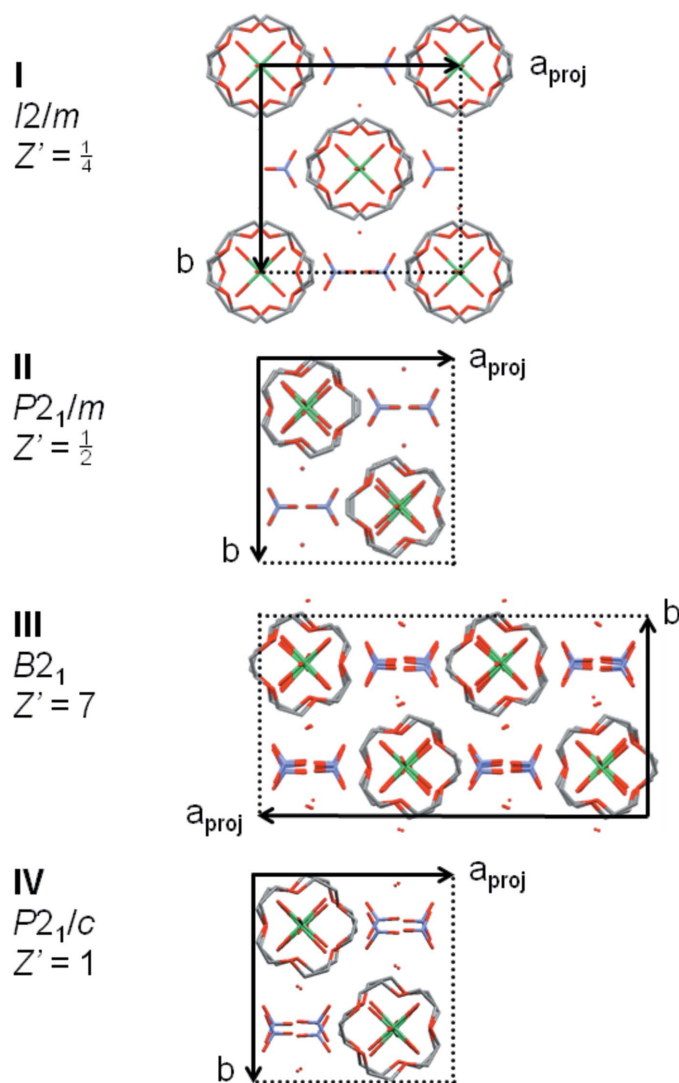


Figure 1
Diagram showing the four phases of $[\text{Ni}(\text{H}_2\text{O})_6](\text{NO}_3)_2 \cdot (15\text{-crown-5}) \cdot 2\text{H}_2\text{O}$ found between 308 K (phase I) and 90 K (phase IV). All cells are shown in projection along c , which points into the drawing; the axes \mathbf{a}^* are in the plane of the drawing while the axes \mathbf{a} point out of that plane. The relative lengths of the c axes are $c_I = c_{II} = c_{III}/7 = c_{IV}/2$. The unit cell of phase I can be made to look even more similar to those of the other phases by shifting its origin by $[\frac{1}{4}, \frac{1}{4}, \frac{1}{4}]$, *i.e.* to a different inversion center. The unit cell of phase III can be made to look even more similar to those of phases II and IV by shifting its origin by $[-\frac{1}{4}, -\frac{1}{2}, -\frac{1}{4}]$, *i.e.* to a different 2_1 axis. The disorder in phase III is shown for the lattice water molecules only.

Fig. 4) with layers of 15C5 molecules; the two types of layers are linked by hydrogen bonds between the cations and the 15C5 molecules shown in Fig. 2.

By looking at this system carefully we hoped to be able to understand the reason for the occurrence of the very unusual modulated phase. A multi-temperature study of the closely related monohydrate $[\text{Ni}(\text{H}_2\text{O})_6](\text{NO}_3)_2 \cdot (15\text{-crown-5}) \cdot \text{H}_2\text{O}$ (Siegler, Parkin, Angel & Brock, 2011), which has just one phase transition between room temperature and 90 K, showed important structural changes with T within one of the phases as well as between phases.

2. Experimental

As reported earlier (Siegler *et al.*, 2008) we found NiW6-2W to be the only product when crystals are grown by room-temperature evaporation of aqueous solutions equimolar in $[\text{Ni}(\text{H}_2\text{O})_6](\text{NO}_3)_2$ and 15-crown-5 (hereafter abbreviated as 15C5). The light green crystals grow as parallelepipeds that are very long in the direction parallel to the $15\text{C5} \cdot \text{H}_2\text{O} - \text{Ni}$ —

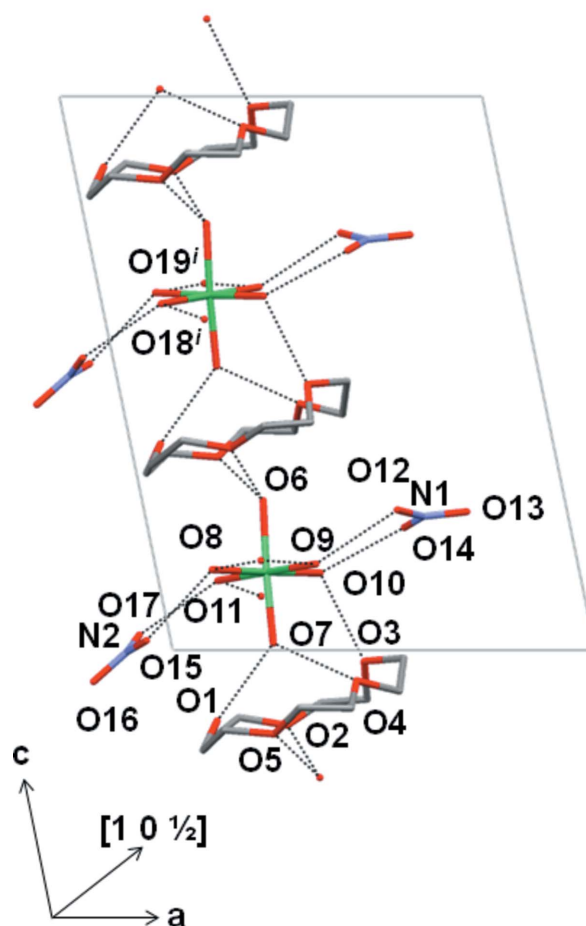


Figure 2
Diagram showing the hydrogen-bonded chain in phase IV of $[\text{Ni}(\text{H}_2\text{O})_6](\text{NO}_3)_2 \cdot (15\text{-crown-5}) \cdot 2\text{H}_2\text{O}$. Atoms labeled O18ⁱ and O19ⁱ have been taken through the symmetry operation $x, -\frac{1}{2} - y, \frac{1}{2} + z$. The numbering around the 15-crown-5 ring is O1—C1—C2—O2—C3—...—C13—O5—C14—C15—. Only the O—H...O bonds involving the cations and the 15-crown-5 molecules are shown.

$\text{OH}_2 \cdots 15\text{C}_5$ hydrogen-bonded chain that runs along c (see Fig. 2). The most prominent crystal faces belong to the form $\{110\}$, where indices are given for the cell with $a \simeq b$ of phases I, II, and IV (see Table 1).

2.1. Differential scanning calorimetry (DSC)

The thermal behavior of the compound was investigated using the DSC 822^e apparatus from Mettler Toledo under control of the software *STARe* (Version 8.10). The DSC samples were prepared from fine powders. For the pair of DSC traces shown in Fig. 5 a sample of 2.9 mg in a pierced Al pan was cooled at a rate of 5 K min^{-1} from room temperature to 173 K, held at that temperature for a few minutes, and then reheated at the same rate to 323 K. Phases were numbered sequentially beginning at room temperature and ending at low temperature (see Figs. 1 and 5).

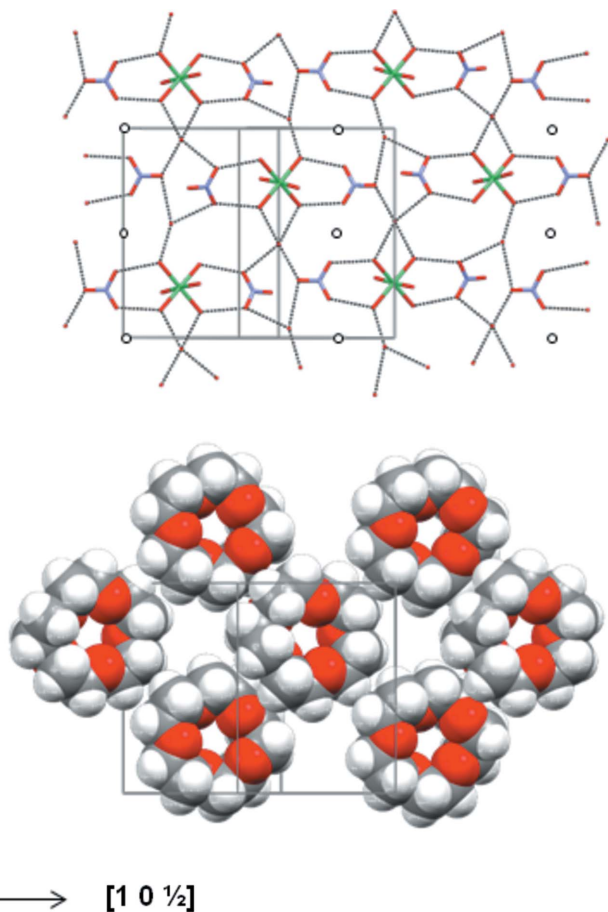


Figure 3

Projections of the hydrogen-bonded and 15-crown-5 layers in phase IV at 90 K. Adjacent hydrogen-bonded and 15C5 layers in that phase are separated by $c/4$. The nitrate ions at the very left of the upper drawing are related by translation to those at the very right, as are the crown molecules on the two sides of the lower drawing. Inversion centers in the hydrogen-bonded layer are marked as are the hydrogen bonds. The layer plane is $(10\bar{2})$ in phase IV; and is $(10\bar{1})$ in phases II and I, where c is half as long. In phase IV each $[\text{Ni}(\text{H}_2\text{O})_6]^{2+}$ ion is the donor in 12 hydrogen bonds; the five that are not shown are to the O atoms of the 15-crown-5 molecules.

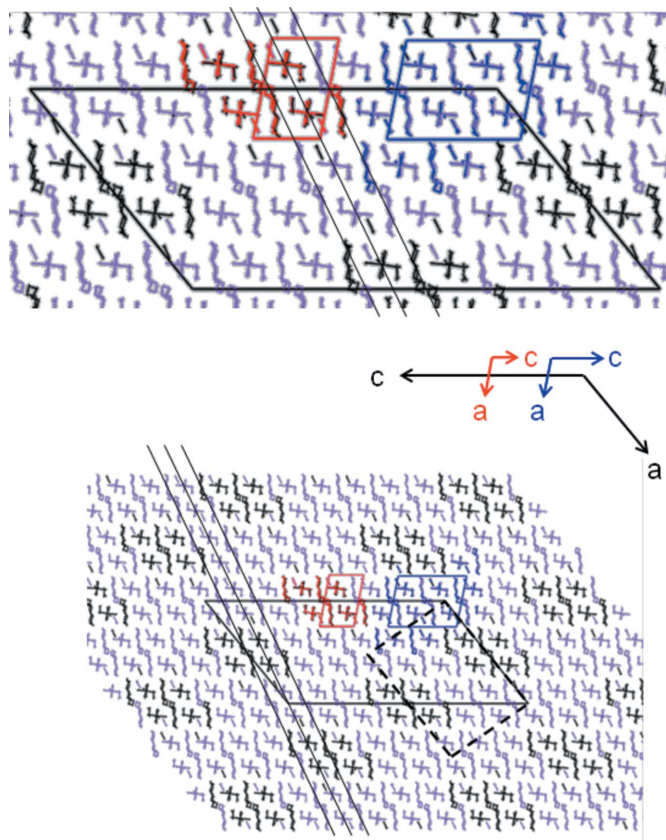


Figure 4

Projection along b of the phase III structure. Formula units 1 and 2, which are like the units in phase II, are colored black; units 3–7, which are like those in phase IV, are colored purple. The larger black cell is for the space group $B2_1$ that was used; the smaller, dashed black cell is for the standard $P2_1$ setting. Small parts of the phase II (red) and phase IV (blue) structures are superimposed on the phase III structure to demonstrate how similar all the phases are. In each drawing the traces of three of the layer planes (two 15-crown-5 layers and a hydrogen-bonded layer; see Fig. 3) are shown.

2.2. Structure determinations

All X-ray data were collected with a Nonius KappaCCD diffractometer equipped with a CRYOCOOL-LN2 low-temperature system (CRYO Industries of America, Manchester, NH). Our calibrations of the CRYOCOOL-LN2 system using $\text{N}_2(l)$, the phase transition in $\text{KH}_2\text{PO}_4(s)$ near 122 K, and an $\text{H}_2\text{O}(s)/\text{H}_2\text{O}(l)$ bath indicate that the temperature precision is 0.2 K and the accuracy no worse than 0.5 K. Mo $K\alpha$ radiation from a fine-focus sealed tube was used. In most cases, and especially at temperatures near the phase transitions, the data in the unintegrated frames were transformed to reconstruct slices nkl , hnl and hkn , $n = 0-3$ of the reciprocal lattice. Small sections of $h0l$ or $h1l$ slices illustrating the changes in the diffraction patterns through the phase transitions are included with the supplementary material.¹

Structures of each of the four phases were initially determined at one temperature (see below and Table 1). Several

¹ Supplementary data for this paper are available from the IUCr electronic archives (Reference: HW5018). Services for accessing these data are described at the back of the journal.

Table 1

Experimental details.

For all structures: $C_{10}H_{20}O_5 \cdot H_{12}NiO_6^{2+} \cdot 2NO_3^- \cdot 2H_2O$, $M_r = 547.12$. Experiments were carried out with Mo $K\alpha$ radiation using a Nonius KappaCCD diffractometer. Absorption was corrected for by multi-scan methods *SCALEPACK* (Otwinowski & Minor, 2006).

	Phase IV at 205 K	Phase III at 90 K	Phase III at 213 K	Phase II at 250 K	Phase I at 294 K
Crystal data					
Crystal system, space group	Monoclinic, $P2_1/c$	Monoclinic, $B2_1$	Monoclinic, $B2_1$	Monoclinic, $P2_1/m$	Monoclinic, $I2/m$
Temperature (K)	205	90	213	250	294
a, b, c (Å)	12.137 (2), 12.635 (2), 16.050 (2)	30.632 (3), 12.594 (1), 55.955 (5)	31.013 (5), 12.560 (2), 56.246 (7)	12.303 (2), 12.543 (2), 8.049 (1)	12.370 (2), 12.570 (2), 8.1140 (1)
β (°)	101.19 (2)	129.46 (1)	129.19 (2)	100.65 (2)	101.48 (2)
V (Å ³)	2414.5 (7)	16666 (4)	16981 (7)	1220.7 (3)	1236.4 (3)
$Z; Z'$	4; 1	28; 7	28; 7	2; $\frac{1}{2}$	2; $\frac{1}{2}$
μ (mm ⁻¹)	0.89	0.90	0.89	0.88	0.87
Crystal size (mm)	0.40 × 0.25 × 0.25	0.60 × 0.25 × 0.20	0.50 × 0.30 × 0.25	0.30 × 0.20 × 0.10	0.35 × 0.30 × 0.05
Data collection					
T_{min}, T_{max}	0.718, 0.808	0.614, 0.840	0.666, 0.809	0.778, 0.917	0.751, 0.958
No. of measured, independent and observed [$I > 2\sigma(I)$] reflections	10 836, 5546, 3493	139 991, 37 869, 16 572	177 757, 38 790, 10 746	5515, 2930, 1883	2838, 1487, 1162
R_{int}	0.044	0.054	0.089	0.040	0.037
Refinement					
$R[F^2 > 2\sigma(F^2)], wR(F^2), S$	0.045, 0.123, 1.00	0.047, 0.154, 1.23	0.060, 0.188, 1.18	0.044, 0.119, 1.00	0.049, 0.131, 1.02
No. of reflections	5546	37 869	38 790	2930	1487
No. of parameters	337	984	1002	345	144
No. of restraints	24	1777	1693	124	31
H-atom treatment	H atoms treated by a mixture of independent and constrained refinement	H-atom parameters constrained	H atoms treated by a mixture of independent and constrained refinement	H atoms treated by a mixture of independent and constrained refinement	H atoms treated by a mixture of independent and constrained refinement
$\Delta\rho_{max}, \Delta\rho_{min}$ (e Å ⁻³)	0.63, -0.55	0.73, -0.59	0.95, -0.90	0.40, -0.44	0.44, -0.33

Computer programs: *COLLECT* (Nonius, 1999), *DENZO-SMN* (Otwinowski & Minor, 2006), *SHELXS97*, *SHELXL97*, *SHELX97* (Sheldrick, 2008), *Mercury* (Macrae *et al.*, 2008), and local procedures.

crystals were studied at 90 K after flash cooling because some such 'single' crystals of phase III contained regions of phase IV. Several crystals were studied at room temperature because in some the phases I and II seemed to coexist.

Later in the study full sets of data were collected at 28 temperatures in the range 90–308 K. The temperature intervals were approximately +10 K except in the regions near the phase transitions, where the intervals were approximately +5 K. Data collection was not started until at least 20 min after the temperature was changed. Data collection took 2.2–3.5 h at most temperatures; a few sets of data were collected somewhat more slowly. More than one crystal was used. The first crystal was cooled slowly to 90 K and data were then measured as a function of increasing temperature to 263 K. The overall R_{merge} value as determined during frame integration changed with exposure time, but was never higher than 0.068. A second crystal was used in the range 253–280 K (overlap with the first crystal at 253 and 263 K). At 285 K and above a new crystal had to be used at each temperature. We conclude that the crystals are damaged somewhat by X-rays, particularly at higher temperatures.

All structures were solved and refined in the same way (see Table 1 and Siegler *et al.*, 2008). The axial systems for phases I, II and III were chosen to make the similarities to phase IV (Steed *et al.*, 2001; Siegler *et al.*, 2008) obvious (see Fig. 1). The atom-numbering schemes were chosen to be as consistent as

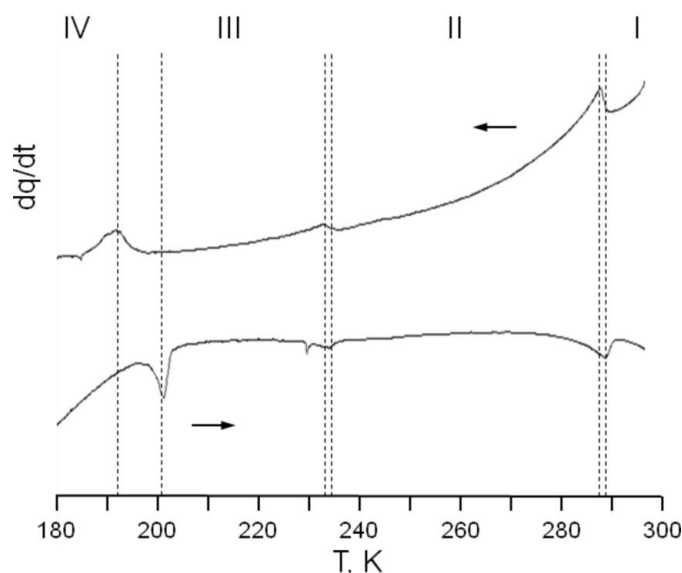


Figure 5
DSC traces for the compound $[Ni(H_2O)_6](NO_3)_2 \cdot (15\text{-crown-5}) \cdot 2H_2O$ measured for both cooling and heating at 5 K min^{-1} . The two traces show three solid–solid phase transitions. We believe the small, sharp feature at ca 230 K in the heating curve and the even smaller feature at ca 185 K in the cooling curve to be artifacts resulting from electronic noise, which is a known problem for the instrument used. The lowest-temperature phase transition shows significant hysteresis. The continuation (not shown) of the heating trace indicates obvious decomposition above ca 295 K as the curve continues to drop off with increasing slope.

possible with that used for phase IV by Siegler *et al.* (2008). During the final refinements the H atoms of the 15C5 ligands were placed at calculated positions [instruction AFIX 23 in *SHELXL97* (Sheldrick, 2008)] with isotropic displacement parameters having values $1.2 \times U_{eq}$ of the attached C atom. The H atoms of water molecules were located (except as noted below) in difference Fourier maps and restrained such that the O–H distances and H–O–H angles had values within accepted ranges [$d(\text{O–H}) = 0.82\text{--}0.84 \text{ \AA}$, $\text{H–O–H} \approx 104.5^\circ$].

Full details of 23 refinements not shown in Table 1 are included with the supplementary material.

2.2.1. Phase IV. This $P2_1/c$, $Z' = 1$ structure is the same as reported earlier at 173 K (Steed *et al.*, 2001) and 90 K (Siegler *et al.*, 2008). It is included in Table 1 at 205 K for comparison

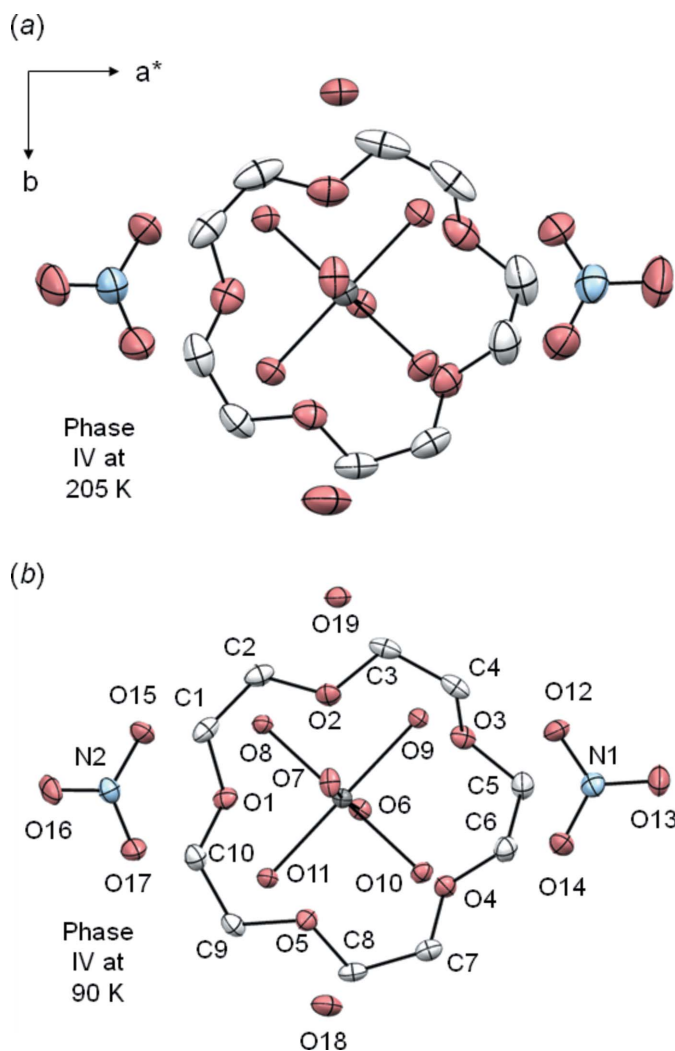


Figure 6
Ellipsoid plot (50% probability level) for one formula unit of phase IV ($P2_1/c$) of $[\text{Ni}(\text{H}_2\text{O})_6](\text{NO}_3)_2 \cdot (15\text{-crown-5}) \cdot 2\text{H}_2\text{O}$ at (a) 205 K and (b) at 90 K, as viewed along **c**. The atom-numbering scheme is shown. Note that the ring shown is not the one to which the O10 shown forms a hydrogen bond (see text and Fig. 2). The O3 atom to which the O10 shown forms a hydrogen bond has coordinates which have been taken through the symmetry operation $x, \frac{1}{2} - y, \frac{1}{2} + z$.

with the structures of phase III at 213 K and of phase II at 250 K.

Refinements of the structure of phase IV were problem-free at all 14 temperatures. The value of R_1 increased slowly from 0.038 at 90 K to 0.045 just below the transition to phase III. There was no indication of disorder. The displacement ellipsoids at 205 and 90 K are illustrated in Fig. 6.

2.2.2. Phase II. When the crystal is warmed through the transitions $\text{IV} \rightarrow \text{III} \rightarrow \text{II}$ the symmetry changes from $P2_1/c$, $Z' = 1$ in phase IV to $P2_1/m$, $Z' = \frac{1}{2}$ in phase II. As phases IV and II are very closely related (see Figs. 1 and 4) we chose a non-standard setting of the $P2_1/m$ cell in which the axes **a** and **c** are interchanged

$$\mathbf{a}'(P2_1/m) = (001/0 - 10/100)\mathbf{a}(P2_1/m)$$

so that its dimensions could be compared easily with those of phase IV. Compared with phase IV, *c* and the cell volume of phase II are approximately halved.

In phase II the nickel cation, the 15C5 molecule and the two nitrate ions are all bisected by a mirror plane perpendicular to **b** (see Figs. 1 and 7). The imposed mirror symmetry requires twofold disorder of at least two atoms of the 15C5 molecule (C5 and C6) because of the incompatibility of the preferred 15C5 conformation with mirror symmetry. A standard anisotropic refinement of a model including disorder of the O3–C5–C6–O3' fragment only (283 adjustable parameters) led to an acceptable agreement factor ($R_1 = 0.054$), but also gave a very eccentric ellipsoid (see figure in the supplementary material) for O7, which is in one of the two 'axial' water ligands in the hydrogen-bonded chain. This eccentric ellipsoid suggested more extensive disorder. The final model ($R_1 = 0.044$; see Fig. 7 and Table 1) includes two mirror-related sites (occupancy 0.5) for the Ni ion, for all of the water ligands except O6, and for all the atoms of the 15C5 molecule except

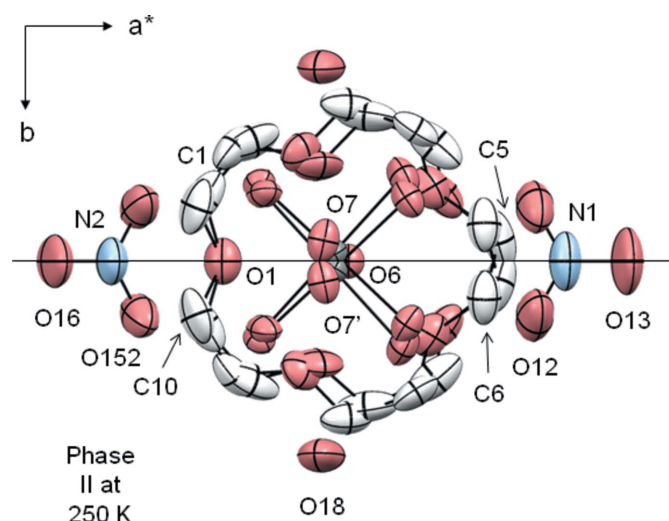


Figure 7
Ellipsoid plot (50% probability level) for one formula unit of phase II ($P2_1/m$) of $[\text{Ni}(\text{H}_2\text{O})_6](\text{NO}_3)_2 \cdot (15\text{-crown-5}) \cdot 2\text{H}_2\text{O}$ at 250 K as viewed along **c**. Part of the atom-numbering scheme, which is basically the same as shown in Fig. 6, is shown. The trace of a crystallographic mirror plane is shown.

O1. Both O1 and O6 are located on the mirror plane. This model also includes restraints on all bonded distances in the cation and 15C5 molecule; target distances and estimated standard deviations were based on the phase IV structure but were shortened slightly because of the increased thermal motion [target distances 1.50 (2) Å for C—C; 1.43 (2) Å for C—O; 2.04 (1) Å for Ni—O_{ax}; 2.05 (1) Å for Ni—O_{eq}; 4.08 (1) Å for O6···O7]. The O—H and 1,3 H···H distances were also restrained. Rigid-bond restraints (instruction DELU) were imposed on all anisotropic displacement parameters (hereafter, ADPs) in the cation and 15C5 molecule. The total number of restraints was 124. The distance between the two sites of the disordered axial O7 atom is 0.82 Å; the distances between pairs of Ni, O8 and O10 atoms are 0.32, 0.36 and 0.55 Å. The ellipsoids for atoms N1 and O13, and maybe N2 and O16, still suggest a large thermal motion in a flat or double-well potential. The ellipsoids for atoms O1 and O6 are consistent with their being ordered.

While this full disorder model could be refined for three fresh crystals studied near 250 K (all cooled slowly from room temperature), use of the model in other situations resulted in large correlations that caused convergence problems and resulted in unsatisfactory displacement ellipsoids. Many disorder models were tried. The one that was the most satisfactory across the full phase-II temperature range allowed for mirror-generated disorder of the O3—C5—C6—O3' fragment only (194 variables total). There were 6 constraints (the U^{ij} values for O3 and O3' were set equal) and 35 restraints (rigid-bond restraints for the atoms of the 15C5 molecule; restraints on the C4—O3/O3', O3—C5, O3'—C6, and C5—C6 bond lengths in the disorder fragment; restraints on O—H and 1,3 H···H distances). The R_1 values are 0.052–0.056 for the three lowest temperatures (253, 263, 273 K), but increase to 0.063, 0.068 and 0.089 at 280, 285, 290 K during the approach to the transition to phase I. The displacement ellipsoids for all atoms other than those of the disordered fragment increase regularly with T until 290 K, where the ellipsoids of the 15C5 ring seem no longer to correspond to a sensible model for thermal motion. The ellipsoids for the disordered fragment are already very large at 280 K.

2.2.3. Phase I. When crystals were warmed through the transition II → I there was no discontinuity in the cell constants but the symmetry increased from $P2_1/m$, $Z = 2$, $Z' = \frac{1}{2}$ to $I2/m$, $Z = 2$, $Z' = \frac{1}{4}$ and the $h + k + \ell$ odd reflections disappeared. The conventional space group for phase I would be $C2/m$, but we chose the $I2/m$ setting because the resulting cell constants are more easily compared with those in phases IV and II. The transformation is given by

$$\mathbf{a}(I2/m) = (101/0 \ -10/00 \ -1)\mathbf{a}(C2/m).$$

In phase I there is $2/m$ symmetry imposed on the cation, which has only two independent O atoms, and on the 15C5 molecule (see Fig. 8), which has three. The twofold axes are perpendicular to the hydrogen-bonded chain and so make the two 'axial' water ligands equivalent. The nitrate ion has imposed symmetry m (two independent O atoms) and the lattice water molecule lies on a twofold axis. The phase I and II structures

look more different than they are (see Fig. 1 and its caption) because of an origin shift between the $P2_1/m$ and $I2/m$ unit cells.

The disorder of the 15C5 molecule, which must assume at least four orientations, is extensive and complicated. The final model (four orientations; refined for data measured at 294, 295 and 303 K) included three O atoms and six C atoms: O1 on the mirror plane with occupancy $\frac{1}{4}$; O2, O3, and C1–C4 on general positions with occupancy $\frac{1}{2}$; and C5 and C6 on general positions with occupancy $\frac{1}{4}$. The 'up–down' disorder of C5 and C6 was imposed because it is required by the incompatibility of the preferred conformation of the 15C5 molecule and the mirror symmetry. All bond lengths in the 15C5 molecule were restrained [targets 1.48 (2) Å for C—C; 1.40 (2) Å for C—O], and rigid-bond restraints (instruction DELU) were imposed on all ADPs. H atoms were added in calculated positions (AFIX 23). It is somewhat surprising that refinement of this model is stable because atoms C2 and C4 are only 0.2–0.3 Å apart at 294–303 K. Any additional disorder in the structure was absorbed into the displacement parameters (see Fig. 8). The ellipsoid for atom O6, which is split into the ordered O6 and the disordered O7 in phase II (see Fig. 7), is neither exceptionally large nor especially elongated.

2.2.4. Commensurate description of phase III. When described as commensurate, phase III has the space group $P2_1$ with $Z' = 7$. The structure is modulated, which is to say that the independent formula units are related by strong pseudosymmetry (here, pseudotranslations and pseudoglide) and that $6/7^{\text{th}}$ of the data are systematically weak. (Wilson plots for groups of reflections $h \ k \ \ell \pm n$, $n = 0-3$, are given with the supplementary material). Data were collected at 90 K, where

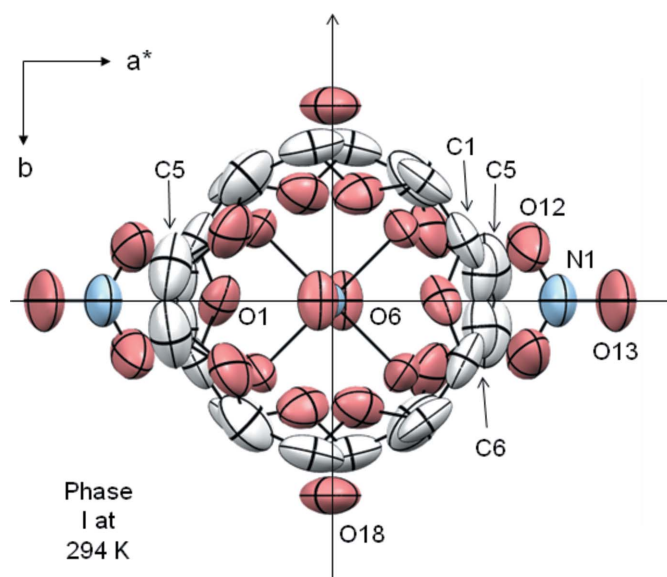
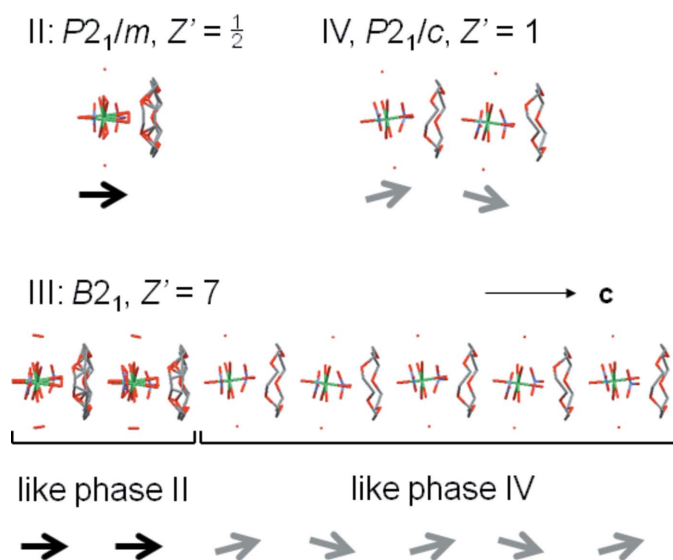
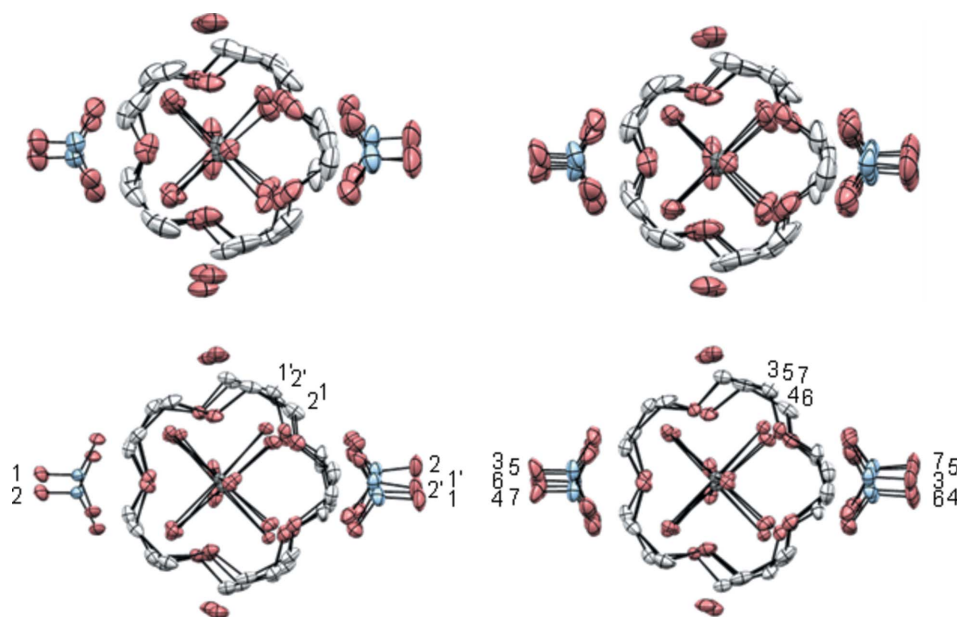


Figure 8 Ellipsoid plot (50% probability level) for one formula unit of phase I ($I2/m$) of $[\text{Ni}(\text{H}_2\text{O})_6](\text{NO}_3)_2 \cdot (15\text{-crown-5}) \cdot 2\text{H}_2\text{O}$ at 294 K as viewed along c . The (superimposed) twofold axes that pass through the cation and through the 15-crown-5 molecule are shown, as is the trace of the mirror plane. Part of the atom-numbering scheme, which is basically the same as shown in Fig. 6, is shown.


Figure 9

Projections of the asymmetric units of phases II, III and IV. The symmetry equivalent of the asymmetric unit for phase IV (*i.e.* a second asymmetric unit generated by the *c* glide) is shown in order to make similarities with phase III obvious. Phase III contains a disordered region of two formula units that is similar to the phase II structure and an ordered region of five formula units that is similar to the phase IV structure. The disorder in phase III is generated by a local pseudomirror. The first two formula units are related by a pseudotranslation of *c*/7; the other formula units are related by a pseudoglide with the same translation. The arrows indicate the average O6–Ni–O7 direction.

phase III is metastable, so that the intensities of the weak reflections would be as great as possible [44% of the data were found to have $I > 2\sigma(I)$]. Data for a different crystal were also


Figure 10

Ellipsoid plots (50% probability level) for the seven formula units in the asymmetric unit of phase III. All units are viewed along **c**. Those in the upper row were determined at 213 K, those in the lower row at 90 K. Formula units 1 and 2 are shown on the left; units 3–7 are shown on the right. The numbers of the formula units are indicated. The atom-numbering scheme is the same as in Fig. 7. Note that while the cation and 15C5 molecule have two basic positions, the positions of the nitrate ions are more variable.

collected carefully (*i.e.* over 10.3 h) at 213 K, which is just above the temperature of the IV \rightarrow III transition, in order to check the similarity of the structures at 90 K and at the low end of the phase III stability range. At 213 K only 28% of the data have $I > 2\sigma(I)$. Small sections of an *h1l* slice illustrating the differences between the diffraction patterns measured at 90 and 213 K are included with the supplementary material.

The structure of phase III was originally solved at 90 K in the noncentrosymmetric space group $P2_1$ [cell constants 21.740 (2), 12.594 (1), 30.632 (3) Å and 96.51 (1)°]. A transformation to the non-standard space group $B2_1$

$$\mathbf{a}(B2_1) = (001/0 - 10/20 - 1)\mathbf{a}(P2_1)$$

was then made so that hydrogen-bonded chains of Ni cations and 15C5 molecules would be parallel to **c**, as they are in the other phases (see Fig. 4). In the standard cell chosen (right-handed coordinate system; obtuse angle β that is as small as possible) the directions of the axes **b** and **c** in the $Z' = 7$ cell are antiparallel to those in the other three cells.

In phase III there are local pseudomirror planes in some regions of the structure and local pseudoglide planes in others. The regions with the local pseudomirror symmetry are disordered in the same way that phase II is disordered. The regions with the local pseudoglide symmetry are very similar to the ordered phase IV (see Fig. 9). The crystallographic models for these two different regions were based on the models refined for phases II and IV. In the phase II regions two cations, two 15C5 molecules and two pairs of lattice waters (residues 1 and 2) are disordered; in the phase IV region the other five sets (residues 3–7) seem to be ordered. Two of the 14 nitrate ions, those containing N1_1 and N1_2, were described as disordered at 90 K; at 213 K only the disorder of the nitrate ion including N1_2 was included.

The geometries of all independent 15C5 molecules, all $[\text{Ni}(\text{H}_2\text{O})_6]^{2+}$ cations and all nitrate anions related by pseudosymmetry were restrained using the SAME instruction, which affects corresponding distances and angles. All H atoms were placed at idealized positions.

It seemed prudent to impose constraints on the ADPs for the atoms related by pseudosymmetry. The EADP instruction, however, could not be used because the pseudo glide and mirror operations require changes in the orientations of the displacement ellipsoids and therefore in the signs of the U^{23} and U^{12} values. Six free variables (FVARs) were used to describe the six U^{ij} values of each of the 32 non-H atoms (7 + 4 + 4 + 15 + 2) in the

$[\text{Ni}(\text{H}_2\text{O})_6](\text{NO}_3)_2 \cdot (15\text{C}5) \cdot 2\text{H}_2\text{O}$ formula unit; 18 more free variables were used to describe the displacements of the minor component of the disordered nitrate ions in residues 1 and 2. The total number of variables used to describe displacements was therefore 210 ($= 32 \times 6 + 18$).

Separate occupancy factors were refined for the disordered $[\text{Ni}(\text{H}_2\text{O})_6]^{2+}$ cations, the one disordered NO_3^- ion, the crown molecule and the two disordered water molecules in residues 1 and 2. At 90 K the ten occupancy factors averaged 0.62 (2) and varied from 0.555 (3) to 0.721 (18). At 213 K the occupancy factors are less well determined but seem to deviate more from 0.5 for residue 1 and perhaps for residue 2 (see table in the supplementary material). The $Z' = 7$ phase is a racemic twin; the twinning was treated using the *SHELXL97* TWIN instruction with the matrix $(-1 \ 0 \ 0 / 0 \ -1 \ 0 / 0 \ 0 \ -1)$. The refined volume fractions (Flack, 1983) are very close to 0.5.

Careful comparisons (see Fig. 10) show that the structure at 90 K, where it is metastable, is very similar (except for some of the occupancy factors) to the structure at 213 K, where phase III is stable. A few more $\text{O} \cdots \text{O}$ contacts are marked at 90 K as likely hydrogen bonds by *Mercury* (Macrae *et al.*, 2008) because the $\text{O} \cdots \text{O}$ distances are smaller than twice the van der Waals radius of oxygen (1.52 Å; Bondi, 1964), but otherwise the structures are difficult to distinguish except by their displacement ellipsoids. The refinement at 213 K, however, was less stable because the supercell reflections were so much weaker, and it had to be damped. A superspace refinement would probably be preferable.

The final refinement of the structure at 90 K was very satisfactory (see Table 1 and Fig. 10). The final least-squares input file is included with the supplementary material. The

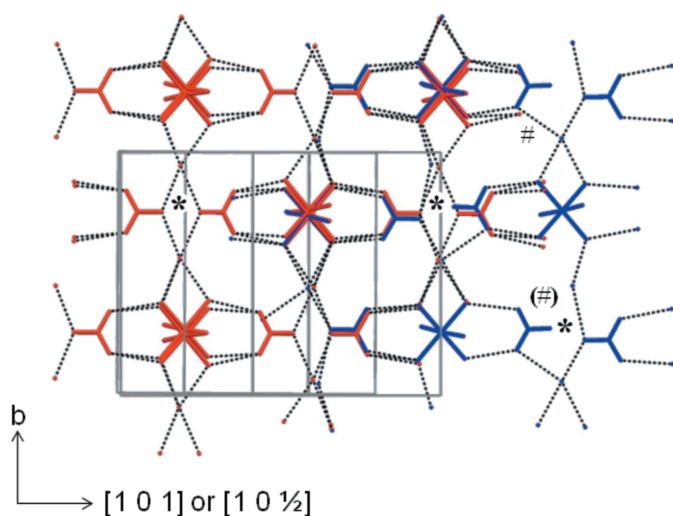


Figure 11

Partial overlay of the hydrogen-bonded layer $(1 \ 0 \ \bar{1})$ of the phase II structure ($P2_1/m$) at 250 K (red) and the corresponding layer $(1 \ 0 \ \bar{2})$ of the phase IV structure ($P2_1/c$) at 205 K (blue). The groupings marked by asterisks are related by translation (red) or a 2_1 axis (blue). The $\text{O} \cdots \text{O}$ contacts shorter than twice the van der Waals radius of oxygen have been marked, but in some cases (notably the $\text{O}_{\text{nitrate}} \cdots \text{O}_{\text{water}} \cdots \text{O}_{\text{nitrate}}$ contacts of the phase II structure) the bonds cannot all be good $\text{O}-\text{H} \cdots \text{O}$ bonds (see text). The $\text{O}_{\text{water}} \cdots \text{O}_{\text{nitrate}}$ contacts in phase IV that are not present in phase II are marked with the symbol #.

largest peaks in the final difference map were located near the nitrate O atoms. The consistency of chemically equivalent bond lengths (which had been restrained) was good; the estimated uncertainties for the averages calculated for the sets of chemically equivalent distances averaged about 1.8 times the average uncertainty of an individual measurement.

2.2.5. Incommensurate description of phase III. After the refinements were essentially complete Dr Rob Hooft, then of Bruker AXS Delft, integrated the original frames measured for phase III at 90 K using the software package EvalCCD (Duisenberg *et al.*, 2003), which allows for incommensurate modulations. He found a basic cell that is very nearly related to the $B2_1$ cell reported here by the matrix $(0 \ 0 \ 1/7 / 0 \ 1 \ 0 / -\frac{1}{2} \ 0 \ -3/14)$; the cell constants for this basic cell (7.990, 12.583, 12.030 Å; 90, 100.77, 90°) are very similar to those of the phase II and phase I structures if the axes a and c are interchanged (see Table 1). If the transformation matrix above premultiplies the cell constants we determined at 90 K for the $B2_1$ setting the resulting basic cell has the dimensions 7.994, 12.594, 12.038 Å and 90, 100.80, 90°. The similarity of these cell constants and those of Hooft's basic cell indicate the two cells have been related correctly.

The modulation vector associated with the basic cell found by Hooft is $q = (0.4302, 0.0001, -0.1312) = (3/7 + 0.0016, 0, -1/7 + 0.0117)$, with uncertainties in the vector components of a little less than 0.001. Since the irrational part of the third

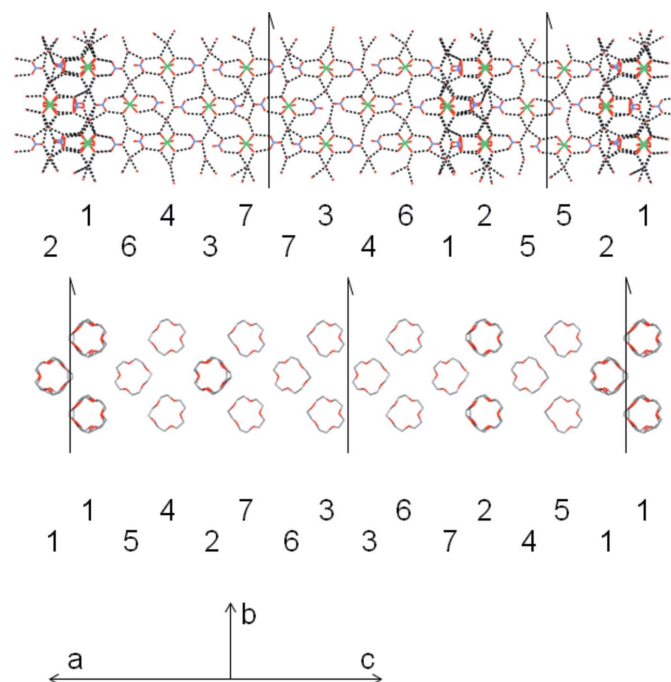
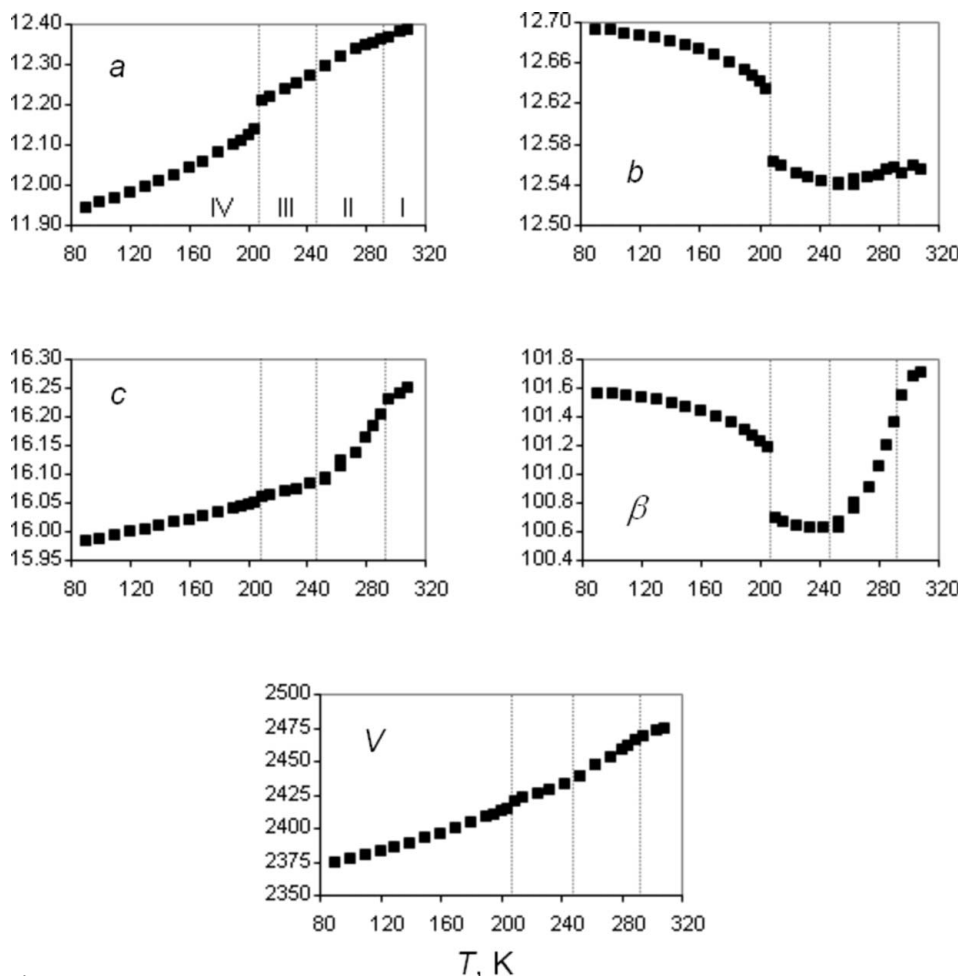


Figure 12

Projections of the hydrogen-bonded and 15-crown-5 layers in phase III at 213 K. The axis \mathbf{b} points upwards and $[1 \ 0 \ 1/7]$ points to the left. The residue numbers of the cations and of the 15-crown-5 molecules are shown. The two parts of the drawing have a common origin so that cations shown in the upper drawing are hydrogen-bonded to the corresponding 15-crown-5 molecules shown in the lower layer. There are 2_1 axes in both layers but they are in different places. A projection of the cell axes on the plane of the drawings is also shown.


Figure 13

Plots of the cell constants a , b , c (Å), β (°) and V (Å³) versus T . The temperatures of the phase changes as determined by the integration of the intensity data are shown; the phase designations are shown only in the first plot. The cell constants have all been brought to a common scale. Phase III was indexed in the $Z' = \frac{1}{2}$ pseudocell; the values c and V were doubled for the phase III pseudocell and for phases I and II. The uncertainties of the values are all smaller than the symbols used. Two sets of values were determined for two different crystals at 253 and 263 K (see text).

component of the q vector, 0.012 (1), is very different from zero the modulation is better described as incommensurate at 90 K, and probably at other temperatures as well.

Transformation of the modulation vector using the matrix $(-3 \ 0 \ -2 \ / \ 0 \ 1 \ 0 \ / \ 7 \ 0 \ 0)$, which is the inverse transpose of $(0 \ 0 \ 1/7 \ / \ 0 \ 1 \ 0 \ / \ -1/2 \ 0 \ -3/14)$, gives q referred to the B_{21} axes as $(-1.028, 0, 3.011)$. If vectors $\pm(-1 \ 0 \ 3)$ are drawn from the main reflections in reconstructed reciprocal-lattice slices $h1\ell$ it is clear (see the supplementary material) that this modulation makes sense of the complicated diffraction pattern. The q vector makes an angle of 0.88° with the B_{21} axis \mathbf{c} .²

The fraction (44%) of reflections found in this integration as having $I > 2\sigma(I)$ at 90 K suggests (because $0.44 = 3/7 + 0.01$) observation of most of the first-order, but many fewer of the second- and higher-order, satellite reflections.

² As the choice of q vector is not unique (see Section 3.9.2 of Smaalen, 2007) the significance of its orientation is limited.

While Hooft's analysis strongly suggests that the modulation is incommensurate we do not think that treating the structure as commensurately modulated has led to any seriously false conclusions because the modulation vector is within a few per cent of being commensurate in the cell used (see Wagner & Schönleber, 2009). Application of chemically reasonable constraints and restraints led to a physically reasonable model that refined well and gave very satisfactory agreement factors. In any event a full refinement of the incommensurate structure, perhaps as a function of temperature, would be a major undertaking that will have to be described in a future paper.

3. Results

3.1. Overview of the structures

The transition I \rightarrow II corresponds to partial ordering associated with a loss of twofold rotation symmetry and a doubling of the asymmetric unit. Further symmetry, most notably the mirror symmetry, is lost in the transitions II \rightarrow III \rightarrow IV, after which the structure is fully ordered and the size of the asymmetric unit again doubled. The structures of phases II and IV are very similar (see Figs. 1, 4 and 11). In the commensurate approximation phase III has a $Z' = 7$

structure intermediate between those of phases II and IV (see Figs. 9 and 12).

All structures are built of alternating layers of 15C5 rings in which there are van der Waals contacts only and hydrogen-bonded layers composed of $[\text{Ni}(\text{H}_2\text{O})_6]^{2+}$ and NO_3^- ions and lattice water molecules (see Fig. 3). The two kinds of layers are linked by hydrogen bonds (see Figs. 2 and 4). The layer planes are $(1 \ 0 \ \bar{n})$, where n is 1, 1, 7 and 2 for phases I–IV. The \mathbf{b} axes lie in the layers, as do the vectors $\mathbf{a} + \mathbf{c}/n$ (i.e. $[1 \ 0 \ 1/n]$).

In all phases the 'axial' water ligands are each hydrogen-bond donors to two ether O atoms in adjacent 15C5 molecules (O6 bonds to O2 and O5; O7 bonds to O1 and O4). In phase IV, and in the ordered regions of phase III, it is clear that the 'equatorial' water ligand containing O10 donates a hydrogen bond to the fifth O atom (O3) of the ring. It seems likely that this $\text{O}_{\text{eq}}-\text{H}\cdots\text{O}_{\text{ether}}$ bond persists in the disordered phase II, but if so, it is disordered by the mirror plane that superimposes O9 and O10.

3.2. DSC traces

The DSC traces (Fig. 5) show that there are phase transitions at *ca* 288, 233 and 196 K. There is minor hysteresis for the two higher-temperature transitions but somewhat larger hysteresis (*ca* 9 K) for the lowest-temperature transition. The $\Delta_{trans}H = \Delta_{trans}S/T_{trans}$ value has the largest magnitude for the transition III–IV and the smallest for II–III, but is always too small to measure reliably.

3.3. Variation of cell constants with temperature

Plots of the cell parameters *versus* *T* are shown in Fig. 13. Phase III data for the temperature sequence were indexed in the $Z' = \frac{1}{2}$ pseudocell because the data were generally not intense enough to allow indexing in the supercell. The values *c* and *V* for the phase-III pseudocell and for phases I and II were doubled to make all cells similar to that of phase IV. At each temperature the best choice for the unit cell and the space-group symmetry was determined during the process of integrating the frames and averaging the reflection intensities. The vertical lines indicate the temperatures at which the space-group symmetry was found to change.

A comparison of Figs. 5 and 13 shows that the phase transition temperatures determined from changes in the diffraction pattern of a single crystal being heated (*ca* 208, 248 and 292 K) are slightly higher than those determined from DSC measurements for a powder being heated (*ca* 201, 234 and 289 K). It is likely that hysteresis is greater for a single crystal with dimensions of *ca* 0.2 mm than for the much smaller crystallites of a powder.

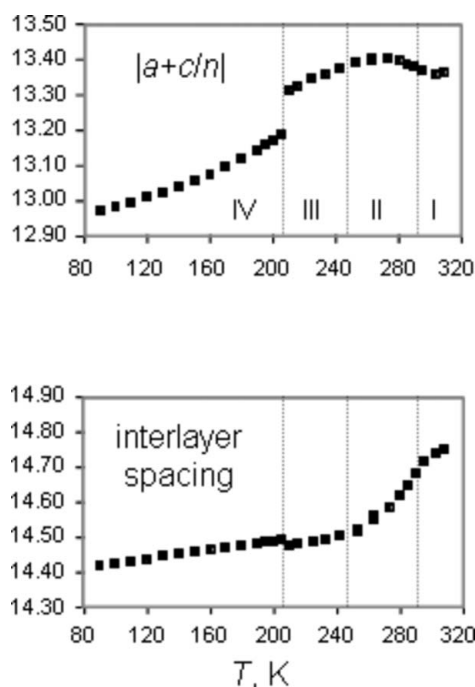


Figure 14

Plots *versus* *T* of the lengths (Å) of $\mathbf{a} + \mathbf{c}/n$ and of the interlayer spacing calculated from $V/[b|\mathbf{a} + \mathbf{c}/n|]$.

The transition between phases IV and III corresponds to clear discontinuities in the cell constants *a*, *b* and β ; these discontinuities are consistent with the much greater hysteresis observed for the IV–III transition than for the other two. There are no obvious discontinuities associated with the other transitions, but there are changes in the derivatives of the curves across the transitions III–II and II–I.

As the structures are layered it is useful to look at thermal contraction within and perpendicular to those layers (see Figs. 3 and 4). The change with *T* of the length $|\mathbf{a} + \mathbf{c}/n|$ and of the interplanar spacing is shown in Fig. 14. There is an obvious discontinuity in the length of $|\mathbf{a} + \mathbf{c}/n|$ through the transition IV \rightarrow III but in the change in the interlayer spacing is less pronounced.

3.4. Differences in hydrogen bonding between phases

It is possible that the hydrogen bonding changes between phases IV and II but in the absence of a neutron-diffraction study the details are necessarily uncertain. Fig. 11 shows the differences in the hydrogen-bonded layer between the highest *T* at which phase IV could be studied (205 K) and the lowest *T* (250 K) at which the structure of phase II could be determined; all $\text{O} \cdots \text{O}$ contacts less than twice the van der Waals radius of oxygen (1.52 Å; Bondi, 1964) are marked. The drawing suggests that each lattice water molecule participates in four hydrogen bonds in phase II but that in phase IV one of the lattice waters participates in only two hydrogen bonds. The marked short contacts, however, are misleading. The angle $\text{O}(\text{nitrate}) \cdots \text{O}(\text{water}) \cdots \text{O}(\text{nitrate}')$ in phase II is only 68° , which means that the lattice water cannot simultaneously make good hydrogen bonds to the two nitrate ions.

The change between 250 and 205 K in the average of the five $\text{O}_{\text{ligand}} \cdots \text{O}_{\text{crown}}$ hydrogen-bonding distances (-0.004 Å; range 2.75–2.82 Å at 205 K) is very small. The average of the other seven $\text{O}_{\text{ligand}} \cdots \text{O}$ distances actually increases with lowered *T*, although not by much ($+0.015$ Å; range 2.70–2.76 Å). The important changes are in the hydrogen bonds made by the lattice water molecules. At 250 K there is probably one $\text{O}_{\text{water}} \cdots \text{O}_{\text{nitrate}}$ interaction per lattice water molecule with a length of 2.82 Å. At 205 K there are two interactions (because there are two independent water molecules) with lengths 2.75 and 2.96 Å, as well as a new $\text{O}_{\text{water}} \cdots \text{O}_{\text{nitrate}}$ interaction of 2.94 Å with a different nitrate O atom. As *T* is lowered to 90 K the third interaction shortens to 2.84 Å and the corresponding (but not drawn) interaction for the other lattice water molecule related by the approximate mirror (see Fig. 3) decreases from 3.20 to 3.04 Å.

3.5. Other changes in the layers between phases

Thermal contraction in phases I and II is concentrated in the interlayer spacing although *b* also decreases slightly. In phase II the length of $[1\ 0\ 1]$ first increases (see Fig. 14) because contraction in that direction is hindered by the $\text{O}13 \cdots \text{O}16$ contact (3.25 Å at 250 K; see the asterisk in Fig. 11), and by contacts of these two O atoms with 15C5 molecules in the adjacent layer. The ellipsoids for the atoms of the two

nitrate ions (O13 and O16) are unexpectedly large and oblate, and thus suggest that the motion of the ions could be correlated.

Between phase II at 250 K and phase IV at 205 K the length of $|\mathbf{a} + \mathbf{c}/n|$, $n = 1$ (phase II) or 2 (phase IV) (see Fig. 14) decreases by 0.21 Å. The interlayer spacing, however, decreases by only 0.03 Å while b increases by 0.09 Å. The overall cell contraction is made possible by the displacement of the two nitrate ions to opposite sides of the mirror planes at $y = \pm \frac{1}{4}$ of the phase II structure (see Fig. 11); the mirror planes in phase II become glide planes in phase IV. The ordering of the 15C5 molecules is also important in the contraction because there are rather short contacts between the disordered 15C5 molecules in phase II.

Phase III is an intermediate phase that has layers (see Fig. 12) in which regions that are like the disordered phase II alternate with regions that are very like the fully ordered phase IV.

3.6. Variations with temperature of individual phases

Phase IV changes very little with T ; the only obvious change is the expansion of the ellipsoids. An overlay made with *Mercury* of all 14 structures (90–205 K) shows essentially no structural changes except for small tilts and shifts of the nitrate ions that cause O13 and O16 to be displaced by *ca* 0.2 Å, and by small shifts (*ca* 0.1 Å) of the lattice water molecules.

The structures of phase III at 90 K, where it is metastable, and at 213 K are also nearly superimposable. Again, very small differences in the positions and orientations of some of the nitrate ions, and even smaller differences in the positions of the water molecules, can be seen, but basically the two structures are the same except for thermal contraction. There are, however, changes in the occupancy factors of the disordered 15C5 molecules and $[\text{Ni}(\text{H}_2\text{O})_6]^{2+}$ cations.

Overlays of the phase II structures suggest that the conformation of the disordered fragment changes slightly with T such that the van der Waals surface of the 15C5 molecule shrinks a little as the temperature increases. The orientations of the nitrate ions also change in a small but regular way. None of the phases shows the kind of significant structural changes with temperature that were observed for the low-temperature phase of the monohydrate $[\text{Ni}(\text{H}_2\text{O})_6](\text{NO}_3)_2 \cdot (15\text{-crown-5}) \cdot \text{H}_2\text{O}$ (Siegler, Parkin, Angel & Brock, 2011).

3.7. Modulations in phase III

While there are only two basic orientations of the 15C5 molecules and $[\text{Ni}(\text{H}_2\text{O})_6]^{2+}$ cations in phase III, Fig. 10 shows that the nitrate ions are modulated in a more complicated way, especially in the regions of the structure in which the cations are ordered. It may be that the modulations of the nitrate ions are key to the complicated phase behavior.

4. Discussion

If there were no phase III this set of structures would be much easier to understand. There are many precedents for a series

of phase transitions during which symmetry is lost while order increases. What is surprising about phase III is its large stability range (*ca* 40 K) and its large unit cell that is a sort of hybrid of the unit cells of phases II and IV. It is also unusual for the size of the asymmetric unit to decrease through a transition as a crystal is cooled as it does in the III \rightarrow IV transition. Desiraju (2007) has described high Z' structures as being 'on the way' between two more conventional phases, but this set of structures is one of the few documented examples of such behavior (but see Chernyshov *et al.*, 2003, and Törnroos *et al.*, 2006).

It seems to be understood that modulated structures (especially high- Z' and incommensurate structures) are often consequences of competing packing requirements (Janssen *et al.*, 2007; van Smaalen, 2007). In that context the alternation of ionic and molecular (*i.e.* 15C5) layers (see Fig. 3 and 4) may be important. It is easy to imagine that the thermal contraction for the two kinds of layers should differ because contraction depends on changes in populations of low-frequency modes, and those modes are different for the two kinds of layers. Looking at the short contacts marked by *Mercury* it appears that the 15C5 layers are less tightly packed than the ionic layers. In the stability range of phase III the complicated modulation observed may be the best compromise possible between the packing requirements for the two different types of layers.

We believe that the hydrogen bonding within the layers (Figs. 3 and 12) is more important to the transmittal of the modulations from one part of the crystal to another than is the hydrogen bonding along \mathbf{c} (Fig. 9). The key to this conclusion is the finding that O6 in phase II, and in the disordered parts of phase III, is ordered. If O6 is in the same position for both cation orientations, then it would seem that the information about the overall ordering along \mathbf{c} cannot be passed easily down the hydrogen-bonded chains that run in a direction approximately parallel to the O6–Ni vector. Within the hydrogen-bonded layers, however, the positions of the nitrate ions, which vary with the tilts and positions of the cations, pass this information along \mathbf{b} and along $[1\ 0\ 1/n]$.

The alternation of the ordered and disordered cations along \mathbf{c} (Fig. 9) in phase III is then a consequence of the alternation pattern within the hydrogen-bonded layer (Fig. 12) and the overall symmetry of the structure. The shifts along \mathbf{b} of the nitrate ions cause similar shifts in the positions of the cations (see Fig. 3). These shifts are then transmitted to the 15C5 molecules in adjacent layers (see Fig. 15), and therefore to the rest of the structure. The $\text{O}_{\text{eq}}\text{—H}\cdots\text{O}_{\text{ether}}$ bond is probably important in transmitting this information because it requires good alignment of the cation and the 15C5 molecule.

Once the phase III structure is established its conversion to the phase IV structure is almost certainly hindered by a mismatch between the deviations of phase III and IV structures from the phase II structure. The largest deviations between these three structures are in the coordinates y . Fig. 15 shows that the variation of $y - \langle y \rangle$ for the Ni ions and for the 15C5 centroids in phase III at 213 K does not match the regular oscillation of these values in the phase IV structure at

205 K. (In the phase II structure these values are all zero if the two disordered positions are populated equally.) Many of the coordinate shifts required for the transition III \rightarrow IV are larger than the average r.m.s. atomic displacement (0.23 \AA at 213 K) calculated from the ADPs. The necessary changes in the tilts of the cations would require even larger displacements.

The suggestion that the modulated phase III is a consequence of the competing packing requirements of two different types of layers is supported by the observation that $[\text{Ni}(\text{H}_2\text{O})_2(\text{MeCN})(\text{NO}_3)_2] \cdot (15\text{C}5) \cdot \text{MeCN}$ (Siegler *et al.*, 2008) goes through a similar series of phase transitions (Siegler, Parkin & Brock, 2011) that includes an intermediate $Z' = 5$ phase. This set of structures is similar to the NiW6-2W structures discussed above in having hydrogen-bonded chains and two different kinds of layers, one containing 15C5 molecules and the other containing the Ni complex. In the MeCN-containing compound, however, there are no strong hydrogen bonds in the layer containing the (neutral) Ni complexes and the acetonitrile solvent molecules. Another similar set of phases is described in Da Silva *et al.* (2010). In that system the phase that is intermediate between disordered and ordered phases has $Z' = 2$, with one disordered and one ordered formula unit.

Further study, including neutron diffraction, to follow the details of the hydrogen bonding, is planned. Large, air-stable crystals can be obtained simply, inexpensively, and reliably, and replacement of the water molecules by D_2O should be easy should the decision be made to study powders.

5. Summary

An unusual sequence of four phases in the range 308–90 K has been characterized for the compound $[\text{Ni}(\text{H}_2\text{O})_6](\text{NO}_3)_2 \cdot (15\text{-crown-5}) \cdot 2\text{H}_2\text{O}$, a compound that can be easily made and studied. Phases I and II, which are the phases stable at the higher temperatures, are related by what seems to be a simple order–disorder transition. Phase III (*ca* 208–248 K) is a modulated structure that has a very large unit cell ($Z' = 7$ if the

structure is described as commensurate) and that has regions that resemble both the disordered phase II and the fully ordered phase IV. The structure of phase III could be determined because a crystal that is cooled very rapidly to 90 K goes through transitions I \rightarrow II and II \rightarrow III, but usually fails to convert to phase IV. At 90 K a large enough fraction of the satellite reflections can be observed that a conventional, if restrained, refinement is possible.

This unusual modulated, intermediate phase may occur because the compound is composed of alternating layers in which the nonbonded contacts differ. The layers composed of 15-crown-5 molecules seem to be rather loosely packed and to have no strong intermolecular interactions. The layers composed of the $[\text{Ni}(\text{H}_2\text{O})_6]^{2+}$ cations, the nitrate anions and the lattice water molecules, however, are held together by strong hydrogen bonds. The thermal contraction properties of these two types of layers must differ, but the layers are linked by $\text{O}_{\text{ether}} \cdots \text{H}_2\text{O} - \text{Ni}$ interactions that require good alignment of the ether molecule and the cation. The modulated phase III is probably a compromise. A similar set of phases has been found for $[\text{Ni}(\text{H}_2\text{O})_2(\text{MeCN})(\text{NO}_3)_2] \cdot (15\text{C}5) \cdot \text{MeCN}$ (Siegler *et al.*, 2008; Siegler, Parkin & Brock, 2011), which is layered in a similar way.

The structure of phase IV does not change much with temperature. The atomic displacement ellipsoids expand as the temperature is raised but the structural changes are minor. The conformation of the 15-crown-5 molecule may change with T in phase II. The temperature dependence of phases I and III could not be determined well, but the occupancy factors for the disordered regions of phase III do differ between 213 K, where the phase is stable, and 90 K, where it is metastable.

M. A. Siegler thanks the University of Kentucky for a 2006–07 Kentucky Opportunity Fellowship. We thank Professor Mark D. Watson of the University of Kentucky Chemistry Department for help with the DSC measurements. We are very grateful to Dr Rob Hooft, formerly of Bruker AXS Delft, for determining how much the phase III structure might deviate from being commensurately modulated.

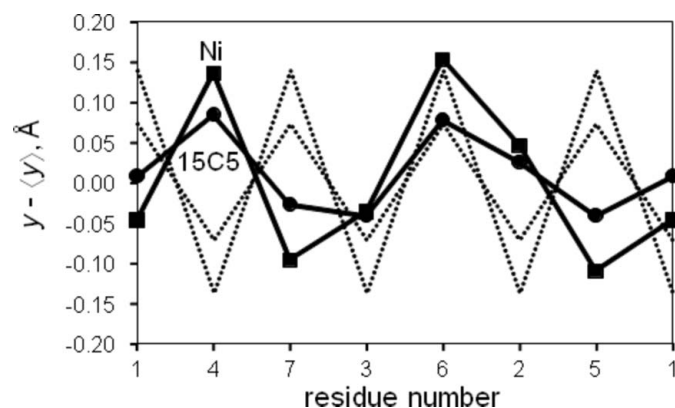


Figure 15
Variation with residue number of $(y - \langle y \rangle)$ for the Ni ion and the 15-crown-5 centroid for phase III at 213 K (solid lines) and phase IV at 205 K (dotted lines). In both cases the deviations are larger for the Ni ion than for the ring centroid.

References

- Allen, F. H. (2002). *Acta Cryst.* **B58**, 380–388.
 Bondi, A. (1964). *J. Phys. Chem.* **68**, 441–451.
 Chernyshov, D., Hostettler, M., Törnroos, K. W. & Bürgi, H. B. (2003). *Angew. Chem. Int. Ed. Engl.* **42**, 3825–3830.
 Da Silva, C. C. P., Martins, F. T., Honorato, S. B., Boechat, N., Ayala, A. P. & Ellena, J. (2010). *Cryst. Growth Des.* **10**, 3094–3101.
 Desiraju, G. R. (2007). *CrystEngComm*, **9**, 91–92.
 Duisenberg, A. J. M., Kroon-Batenburg, L. M. J. & Schreurs, A. M. M. (2003). *J. Appl. Cryst.* **36**, 220–229.
 Flack, H. D. (1983). *Acta Cryst.* **A39**, 876–881.
 Janssen, T., Chapuis, G. & de Boissieu, M. (2007). *Aperiodic Crystals*. IUCr Monographs on Crystallography 20. Oxford University Press.
 Macrae, C. F., Bruno, I. J., Chisholm, J. A., Edgington, P. R., McCabe, P., Pidcock, E., Rodriguez-Monge, L., Taylor, R., van de Streek, J. & Wood, P. A. (2008). *J. Appl. Cryst.* **41**, 466–470.
 Nonius (1999). *COLLECT*. Nonius BV, Madison, Wisconsin, USA.

- Otwinowski, Z. & Minor, W. (2006). *International Tables for Crystallography*, Vol. F, ch. 11.4, pp. 226–235. Heidelberg: Springer.
- Sheldrick, G. M. (2008). *Acta Cryst.* **A64**, 112–122.
- Siegler, M. A., Parkin, S., Angel, R. J. & Brock, C. P. (2011). *Acta Cryst.* **B67**, 130–143.
- Siegler, M. A., Parkin, S. & Brock, C. P. (2011). In preparation.
- Siegler, M. A., Parkin, S., Selegue, J. P. & Brock, C. P. (2008). *Acta Cryst.* **B64**, 725–737.
- Steed, J. W., Sakellariou, E., Junk, P. C. & Smith, M. K. (2001). *Chem. Eur. J.* **7**, 1240–1247.
- Törnroos, K. W., Hostettler, M., Chernyshov, D., Vangdal, B. & Bürgi, H.-B. (2006). *Chem. Eur. J.* **12**, 6207–6215.
- van Smaalen, S. (2007). *Incommensurate Crystallography*. IUCr Monographs on Crystallography 21. Oxford University Press.
- Wagner, T. & Schönleber, A. (2009). *Acta Cryst.* **B65**, 249–268.